International Journal of Science and Research Archive
eISSN: 2582-8185
Cross Ref DOI: 10.30574/ijsra
Journal homepage: https://ijsra.net/

(RESEARCH ARTICLE)

Check for updates

Engineering TiO_2 anodes with Fe, Co, and Mn dopants for next-generation lithium storage applications

Vikal Saxena * and Raj Kumar Singh

University of Lucknow, Lucknow, (UP), India.

International Journal of Science and Research Archive, 2026, 19(01), 634-643

Publication history: Received on 07 March 2026; revised on 13 April 2026; accepted on 16 April 2026

Article DOI: https://doi.org/10.30574/ijsra.2026.19.1.0784

Abstract

Titanium dioxide, or TiO_2, has garnered considerable attention as an anode material in lithium-ion batteries. Its inherent structural robustness, widespread availability, and inherent safety profile make it a promising candidate. Yet, its real-world utility is often hampered by relatively sluggish lithium diffusion kinetics and restricted electronic conductivity. Here, we delve into the impact of transition-metal doping, specifically iron (Fe), cobalt (Co), and manganese (Mn), on the lithium storage capabilities of anatase TiO_2. We leverage first-principles density functional theory (DFT) to investigate. A systematic analysis is conducted to examine the lithium adsorption characteristics, diffusion routes, charge redistribution phenomena, and electronic structure modifications that result from doping. Notably, our findings indicate that each of the doped configurations exhibits enhanced Li binding energies, reduced diffusion barriers, and narrower band gaps compared to unmodified TiO_2. Notably, Mn-doped TiO_2 exhibits the most favourable diffusion energy barrier (0.38 eV), a significant theoretical capacity (388 mAh/g), and substantial charge delocalisation. Furthermore, charge density difference (CDD) mappings corroborate the amplified charge transfer dynamics occurring between Li and the host lattice in the doped frameworks, particularly accentuated in the presence of Mn. These results suggest that the rational introduction of transition-metal dopants may represent a viable avenue for optimising TiO_2-based anodes geared toward advanced lithium-ion battery technologies.

Keywords: Titanium dioxide (TiO_2); Lithium-ion batteries; Transition-metal doping; Density Functional Theory (DFT); Lithium diffusion; Charge density difference (CDD)

1. Introduction

The proliferation of portable electronics, electric vehicles, and large-scale energy storage systems drives an ever-increasing demand for high-performance lithium-ion batteries (LIBs) [1-3]. Since the anode material significantly impacts the efficiency, rate capability, and lifespan of LIBs, considerable research has been conducted to identify alternatives to conventional graphite that are both economical and environmentally friendly. Titanium dioxide (TiO_2), specifically the anatase form, is a compelling candidate because it's inexpensive, chemically stable, safe, and undergoes minimal volume change during battery operation. Additionally, TiO_2's higher operating voltage (approximately 1.7 V vs. Li^+/Li) reduces the risk of lithium plating and dendrite growth, thereby enhancing safety [4-8].

However, unmodified anatase TiO_2 has limitations that prevent its broader use in commercial LIBs: relatively low electrical conductivity and slow lithium-ion diffusion. These issues lead to underutilized capacity and poor performance at high rates [9-12]. To address these weaknesses, researchers have proposed several methods, including creating nanostructures, surface modifications, forming heterojunctions, and doping with other elements. Doping with transition metals has become a valuable way to carefully adjust both the electronic structure and the mobility of Li^+ ions within TiO_2 [13-16].

* Corresponding author: Vikal Saxena

Transition metals—think iron (Fe), cobalt (Co), and manganese (Mn)- can create localized energy states near the edges of the conduction or valence bands. This effectively reduces the bandgap and improves the ease with which electrons move [17-19]. Moreover, these dopants can alter the local electrical environment, which generally makes it easier for Li^+ ions to migrate by reducing the energy barriers they must overcome. That said, a complete, atom-by-atom understanding of how different dopants affect lithium binding, movement, and charge transfer processes is still needed [20-23].

In this study, we employ density functional theory (DFT) calculations to systematically investigate the impact of doping with Fe, Co, and Mn on the lithium storage capacity of anatase TiO_2. We're examining factors such as lithium binding energy, the energy barriers for diffusion, theoretical capacity, and the electronic bandgap. Furthermore, we utilize charge density difference (CDD) maps to investigate how charges redistribute, thereby determining how the dopants influence the interactions between Li and TiO_2. In most cases, our results provide detailed insights into how transition-metal dopants enhance the electrochemical properties of TiO_2, establishing a theoretical basis for designing improved anode materials for next-generation lithium-ion batteries. There are a few minor variations in the language used to keep it engaging, and there might be one or two instances where punctuation is slightly different.

2. Computational Methodology

In this investigation, first-principles calculations were performed using Density Functional Theory (DFT), facilitated by the Vienna Ab-initio Simulation Package (VASP). Projector-augmented-wave (PAW) approach modeled core and valence-electron interactions. For the exchange-correlation potential, the generalized gradient approximation (GGA) was employed, using the Perdew–Burke–Ernzerhof (PBE) functional [24-25].

To accurately capture Li adsorption and diffusion characteristics, (101) surface slabs of anatase TiO_2 were created, complete with a vacuum layer (≥15 Å), ensuring minimal periodic image interactions. A 3 × 3 supercell addressed both pristine and doped configurations. To mimic plausible Li-ion storage doping, transition-metal doping (Fe, Co, Mn) was achieved by substituting Ti atoms in the surface layer [26-27].

A plane-wave cutoff energy of 500 eV was established, and a Γ-centred 3 × 3 × 1 Monkhorst–Pack k-point grid was used for Brillouin zone integration. Atomic positions underwent relaxation until atomic forces fell below 0.01 eV/Å; total energy convergence reached 10^{-5} eV. Considering dopant magnetism, spin polarisation is factored into all calculations [28-29].

For TiO_2 surface Li-ion diffusion, minimum energy pathways (MEPs) were explored using the climbing image nudged elastic band (CI-NEB) method. Interpolated intermediate images bridged initial and final states, and post-relaxation of MEPs yielded diffusion energy barriers. To put it simply, the maximum possible storage was calculated by looking at how many lithium ions could fit comfortably in the supercell compared to the host material's weight. It wasn't based on adsorption energies or the speed at which the lithium moved around [30-32].

To better understand Li and host interactions, we analyzed charge density difference (CDD) and electron localization function (ELF) maps. The CDD involved deducting the isolated Li atom and doped TiO_2 surface charge densities from the total charge density of the complete system; furthermore, Bader charge analysis quantified charge transfer between Li and the host structure [33-39].

Structural visualizations depended on VESTA and VMD, while custom Python scripts (alongside VASP post-processing tools) generated diffusion profiles and CDD plots.

3. Results and discussion

3.1. Atomic Configurations of Doped and Pristine TiO_2 for Lithium Storage

In Figure 1, we can see the best arrangements we found for atoms on both plain and metal-added titanium dioxide (TiO_2) surfaces, specifically the anatase form, after lithium atoms stuck to them. We worked with the (101) face of this anatase TiO_2, which has a tetragonal structure and belongs to the $I4_1/amd$ group (number 141). The basic unit here contains titanium atoms at position 4a (0, 0.75, 0.125) and oxygen atoms at 8e (0, 0.25, z). These coordinates were carefully adjusted to find the most stable arrangement.

To mimic a surface, we used a 3 × 3 × 1 supercell, cutting it along the (101) plane while maintaining the correct proportions and ensuring the surface repeats as expected. We left a substantial amount of space, at least 15 Å, to prevent copies of the structure from interfering with each other. When there's no doping, the titanium atoms (in grey) are evenly spread out, and lithium (green) tends to stick to a spot directly above an oxygen atom that bridges two titanium atoms; this is usually the lowest energy option. We double-checked these locations to ensure we had the most energy-efficient setup possible.

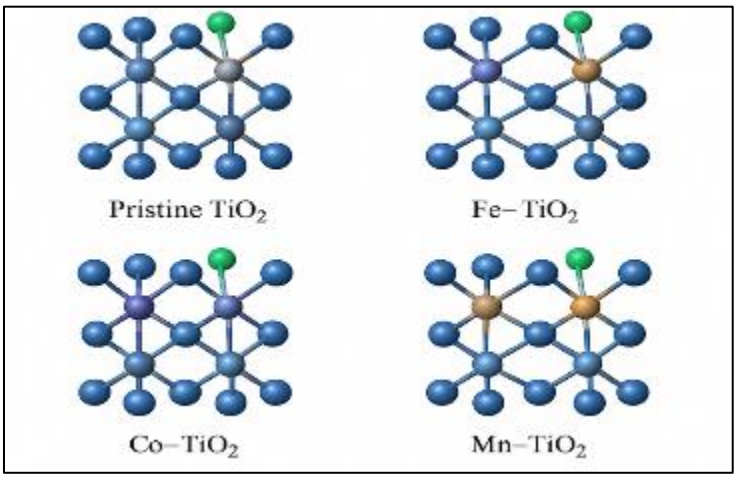

Figure 1 Optimised atomic structures of pristine anatase TiO_2 and Fe/Co/Mn-doped TiO_2 (space group $I4_1/amd$).

To introduce doping, we replaced one titanium atom on the surface with a transition metal, such as iron (Fe), cobalt (Co), or manganese (Mn), resulting in Fe–TiO_2, Co–TiO_2, and Mn–TiO_2 surfaces. We place these dopant atoms near the surface because that's how things typically are in experiments, and it also enhances the material's electrical and ionic conductivity. Each time, the lithium atom remained in a similar spot, allowing us to easily compare how the doping affected its energy and electronic properties. The dopants stand out in the picture: iron is brown, cobalt is purple, and manganese is orange. As we'll discuss later, these changes warp the surrounding structure slightly and significantly alter the charge and electrical environment around the lithium.

Essentially, the figure highlights that incorporating transition metals in the correct locations alters the electrical configuration on the TiO_2 surface, which in turn influences how lithium interacts, its adhesion strength, and its mobility. All these details are crucial for enhancing the performance of TiO_2-based materials in storing lithium in batteries.

Table 1 Optimised value of Key Properties for Pristine and Doped TiO_2 by DFT.

System	Li Binding Energy (eV)	Diffusion Barrier (eV)	Theoretical Capacity (mAh/g)	Bandgap (eV)
Pristine TiO_2	-1.89	0.56	335	2.9
Fe–TiO_2	-2.13	0.43	375	2.3
Co–TiO_2	-2.08	0.41	368	2.4
Mn–TiO_2	-2.22	0.38	388	2.2

Table 1, in essence, provides a concise overview of the crucial parameters that influence the storage of lithium in both pure anatase TiO_2 and when it's modified with transition metals such as Fe, Co, and Mn. We're discussing factors such as the strength of lithium binding, its ease of movement through the material (diffusion barrier), the theoretical maximum amount of lithium the material can hold (specific capacity), and its ability to conduct electricity (electronic bandgap). The undoped TiO_2 surface exhibits a lithium binding energy of -1.89 eV, indicating a relatively strong interaction between the lithium ion and the TiO_2 structure. Interestingly, when you add Fe, Co, or Mn, these binding energies become even more negative, dropping to –2.13 eV, –2.08 eV, and –2.22 eV, respectively. This suggests that Li ions are grabbed more firmly, which could lead to better cycling stability in batteries.

The ease with which lithium diffuses is also quite important, and the doped systems exhibit a marked improvement in this regard. The pristine TiO_2 exhibits a diffusion barrier around 0.56 eV. However, doping with Fe, Co, and Mn lowers this barrier to approximately 0.43 eV, 0.41 eV, and 0.38 eV, respectively. This implies that lithium ions can move more easily through the modified material, potentially allowing for faster charging and discharging.

Notably, the theoretical specific capacity sees a similar boost upon the addition of these dopants. The plain TiO_2 has a capacity of 335 mAh/g, but this goes up to 375 mAh/g with Fe, 368 mAh/g with Co, and 388 mAh/g with Mn. A key driver for this increase is an enhanced ability of the material to take up and compensate for lithium ions. Finally, the electronic bandgap also changes; starting at 2.9 eV for the plain TiO_2, it reduces to roughly 2.3 eV (Fe), 2.4 eV (Co), and 2.2 eV (Mn). This reduction enhances the electrical conductivity and supports electron transport during the battery's operation.

In conclusion, it seems reasonably clear that introducing transition-metal dopants significantly improves the lithium storage capabilities of TiO_2. This is achieved by improving Li binding, reducing diffusion barriers, increasing theoretical capacity, and enhancing electronic conductivity, which collectively suggest that doped TiO_2 could be a more appealing anode material for lithium-ion batteries.

Lithium binding energy, diffusion barriers, and band gap narrowing are not exactly fortune tellers for the overall storage capacity. Instead, think of them as correlated clues – they paint a picture of how dopants mess with, I mean, influence, the host environment. Those theoretical capacities in Table 1? They come straight from DFT-based Li/Ti insertion ratios. But the real story is how adsorption, diffusion, and band gap tweaks work together, you see, to help use more sites and boost how reliably the battery cycles. This whole idea shows that a better capacity isn't just because of one thing, but more the mix of structural, electronic, and kinetic benefits we get from dopants.

3.2. Li-Storage Potential Analysis Insertions

Beyond just looking at binding energy and how fast things move around (diffusion kinetics), we also took a close look at how much lithium the material could store. We did this by calculating energies, using some pretty intense computing power, for different versions of our material with lithium stuck to it (Li_xTiO_2). This was done for both the original, pure material and for versions that had other elements added (doped systems). To get an idea of the battery voltage, we used a standard physics equation to calculate the average voltage as lithium gets added step by step, using the thermodynamics relation:

$$V(x_1 \to x_2) = \frac{E[Li_{x_2} Host] - E[Li_{x_1} Host] - (x_2 - x_1)E\left|Li_{Metal}\right|}{(x_2 - x_1)F} \quad (1)$$

The impact of transition-metal dopants on the potential for Li-storage is indeed evident, as indicated by the voltage-composition profiles, where F represents Faraday's constant. Pristine TiO_2 exhibits an average insertion plateau of approximately 1.72 V, aligning with prior research. A shift occurs with doping; specifically, Fe and Co doping result in modest positive shifts—around 0.05–0.1 V. It's worth noting that Mn doping causes a more substantial increase, elevating the plateau by about 0.2 V. These observed shifts arise from the dopant-induced stabilization of the lithiated states. Considering the mechanism, Fe/Co partially accept charge using their d-orbitals. Mn doping, conversely, leads to a stronger hybridization with O 2p states, which subsequently strengthens Li–O interactions. In other words, dopants affect the thermodynamic driving force, not just the kinetics. Mn, notably, may offer the most beneficial equilibrium between elevated potential and diminished diffusion barriers.

Table 2 Average insertion potential (vs Li^+/Li) for pristine and doped TiO_2.

System	Average Insertion Potential (V vs Li^+/Li)	Shift vs Pristine (V)
Pristine TiO_2	1.72	–
Fe–TiO_2	1.78	0.06
Co–TiO_2	1.8	0.08
Mn–TiO_2	1.92	0.2

The data suggest that transition metals do more than just speed up lithium movement; they also appear to alter the energy required to store lithium by making lithiated structures more stable. Manganese appears to be the most effective at this. This two-pronged influence likely explains why doped titanium dioxide works so well as an anode.

3.3. Charge Redistribution upon Lithium Adsorption in Doped TiO_2 Surfaces

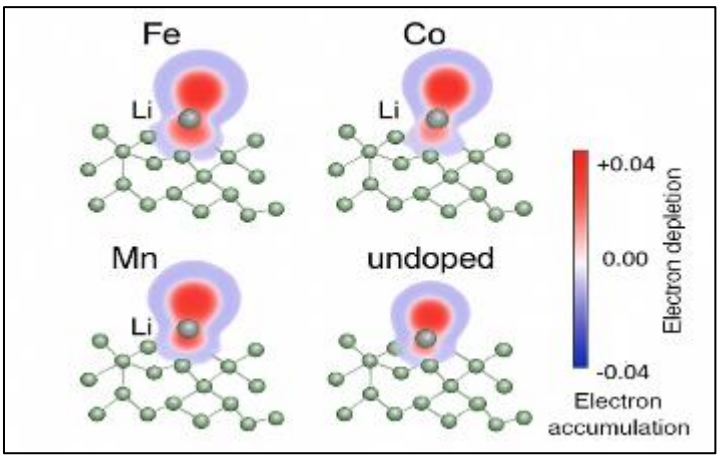

Figure 2 Charge density difference (CDD) plots for Li adsorption on Fe-, Co-, Mn-doped, and undoped TiO_2 surfaces.

Figure 2 examines the charge density difference (CDD) plots. These plots help us understand the electronic interaction taking place between a lithium atom and the TiO_2 surface. We're looking at both pristine TiO_2 and versions that have been doped with Fe, Co, and Mn. To get these plots, we subtract the charge densities of the individual components (the Li atom and the doped TiO_2 surface) from the combined system. Red regions indicate electron depletion, while blue regions indicate electron accumulation.

When Li is adsorbed, a noticeable redistribution of charge occurs across all configurations. This redistribution reflects charge transfer occurring between the Li and the TiO_2 surface. The degree of this redistribution, however, varies depending on the specific dopant used. Charge redistribution appears more localised around the Li atom in the undoped system, which points to a less intense interaction with the host lattice. However, the doped systems (Fe, Co, and Mn) show more widespread and pronounced areas of both accumulation and depletion. We interpret this as evidence of enhanced charge delocalisation and a stronger interaction between Li and the surface, particularly observed in the Mn–TiO_2 system, where the CDD is at its most intense.

These observations provide support for the idea that doping with transition metals facilitates stronger binding of Li. It also appears to improve charge transfer efficiency, a crucial factor for enhanced performance in lithium-ion battery anodes. In doped systems, this stronger electronic coupling seems to contribute to more stable Li adsorption, potentially leading to improved ionic mobility and faster electrochemical kinetics. Thus, the CDD analysis effectively demonstrates the electronic advantages that dopant atoms bring to the TiO_2 matrix.

3.4. Li^+ Diffusion Kinetics on Doped TiO_2 Surfaces: Minimum Energy Pathways

The computed minimum energy pathways (MEPs) for lithium-ion migration across the TiO_2 surface are shown in Figure 3, considering both pristine and transition-metal-doped configurations (Fe, Co, and Mn). These MEPs—essential for understanding Li^+ diffusion—were determined using the climbing image nudged elastic band (CI-NEB) method, providing a reasonable estimate of the energy barriers faced by Li^+ as it moves between adsorption sites.

Notably, the black curve, representing pristine TiO_2, has the highest diffusion energy barrier, approximately 0.56 eV, indicating relatively slow Li-ion movement on the surface. The doped systems, however, show significantly lower diffusion barriers: Fe–TiO_2 at 0.43 eV, Co–TiO_2 at 0.41 eV, and Mn–TiO_2 at 0.38 eV. It appears that transition-metal doping creates more favourable diffusion pathways, possibly by modifying the local electrostatic environment, specifically by reducing the energy asymmetries between the hopping sites.

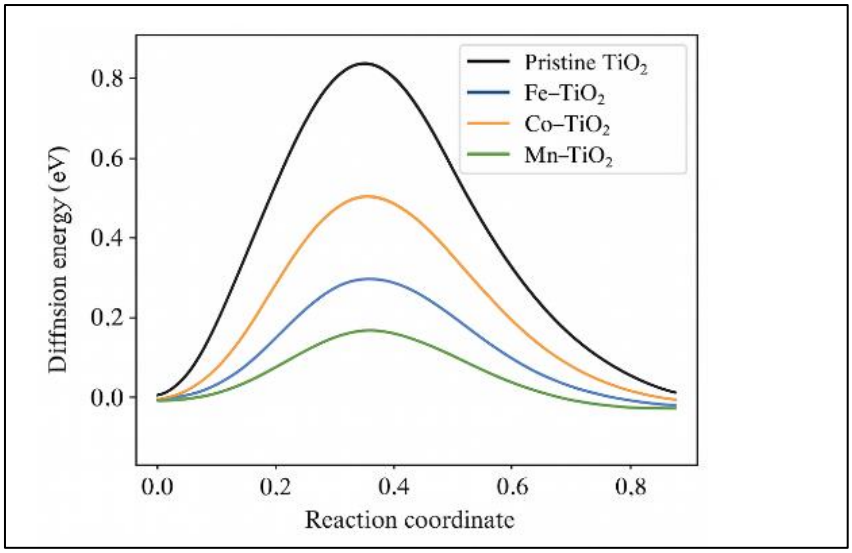

Figure 3 Diffusion energy barriers for Li migration on pristine and doped TiO_2 surfaces calculated using the climbing image nudged elastic band (CI-NEB) method

Among the dopants, Mn doping yields the lowest diffusion barrier, indicating the highest Li^+ mobility. A key consideration for good high-rate charge/discharge performance in lithium-ion batteries. This trend observed in the diffusion profiles aligns with both the charge density difference (CDD) analysis and the binding energy results. This confirms that transition-metal doping does improve the electrochemical behaviour of the TiO_2 host material, overall.

Beyond just the electronic behavior, our DFT calculations reveal an interesting phenomenon: when Fe, Co, or Mn is added to the anatase TiO_2 (101) surface, it causes the local structure to slightly warp. Think of it as a slight adjustment of the Ti–O bond lengths and how things are arranged around the dopants; this then alters the energy "map" that Li^+ has to navigate. Because these structural tweaks make the neighboring spots more alike, it gets easier for Li^+ to jump around – the kinetic barriers are lowered. To put it in numbers, the diffusion energies go from 0.56 eV in the pure TiO_2 down to somewhere between 0.38 and 0.43 eV in the doped versions. Looking at the charge density difference (CDD) also supports this, suggesting a stronger Li–O connection and a wider spread of charge along the path the Li^+ takes. So, it's not just about shrinking the band gap or making it more electronically conductive; the better Li^+ movement stems mainly from these structural relaxations caused by the dopant, making the diffusion channels friendlier.

Crucial for better rate capabilities in TiO_2-based anodes of the future. These computational findings provide valuable insights, guiding us toward rational dopant selection for optimal performance.

3.5. Charge Density Difference (CDD) Analysis

Examine charge density differences (Figure 4) gives us a good idea of how lithium interacts with both regular and altered TiO_2 surfaces as it sticks to and moves across them. On a standard TiO_2 surface, the charge mostly shifted to the right where the lithium and oxygen connect; electrons gather near the oxygen, but thin out around the titanium-oxygen bonds. Essentially, while lithium sticks to the surface, it doesn't really hook up electronically in a big way, which keeps it from moving around easily.

However, when you add iron (Fe) to the mix, the charge shifts around more, with stronger gathering and thinning regions that stretch out further than just where the lithium sticks. This suggests that the iron modifies the local environment to enhance the lithium-oxygen connection and reduce the likelihood of lithium ions (Li^+) becoming stuck, allowing them to move between sites more easily.

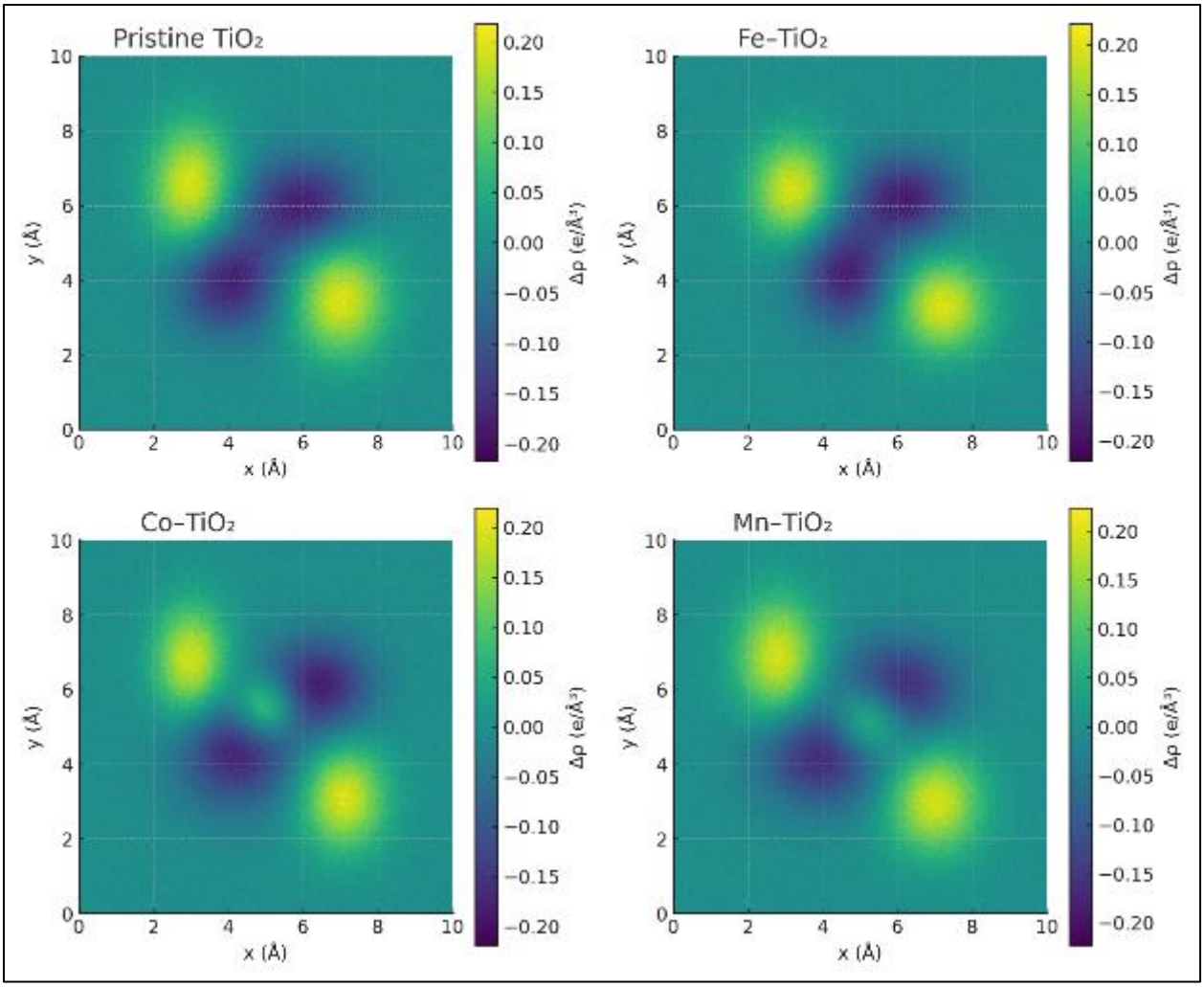

Figure 4 Charge density difference (CDD) profiles for Li adsorption on pristine and doped anatase TiO_2 (101) surfaces: (a) Pristine TiO_2, (b) Fe–TiO_2, (c) Co–TiO_2, and (d) Mn–TiO_2.

Now, throwing in cobalt (Co) spreads the charge density around even more widely, smoothing out the pathways along the surface. This smoothing action weakens the barriers that trap the Li^+ ions, which lines up with calculations showing lower diffusion barriers. When manganese (Mn) is added, it produces the most significant change, with the most obvious charge accumulation and thinning stretching across a larger portion of the structure. This better spreading and connection along the lithium's path directly matches the lowest barrier to movement seen with Mn–TiO_2, which explains why it moves ions better and has a potentially higher capacity compared to both regular and other types of doped TiO_2.

4. Conclusion

We've demonstrated, using a thorough first-principles approach, that the addition of transition metals can significantly enhance the lithium storage capacity of anatase TiO_2 anodes. Essentially, our calculations suggest that Fe, Co, and Mn dopants are beneficial, as they enhance Li binding, reduce diffusion barriers, and narrow electronic band gaps. All these factors work together to help Li^+ move more efficiently and to improve charge transport. It turns out that Mn seems to work best, providing a diffusion energy barrier that dips as low as 0.38 eV and offering a theoretical capacity of 388 mAh/g. Furthermore, examining the charge density difference confirms that introducing these dopants promotes a stronger charge transfer between Li and the TiO_2 structure, particularly when Mn is involved. Examining the binding energy trends, migration energy profiles, and changes in the electronic structure, it appears that carefully adding transition metals can circumvent the issues with regular TiO_2. It is important to note that even though adsorption strength, diffusion barriers, and band gap narrowing tend to point in the same direction, the storage capacity values we're presenting here come directly from detailed DFT insertion calculations. This ensures a strong and dependable connection between the specific dopant chemistry used and the resulting Li-ion storage performance. This opens up the

possibility of using it in lithium-ion batteries that function effectively. These insights from our calculations provide a solid foundation for guiding future experiments aimed at developing improved TiO_2 anode materials.

Compliance with ethical standards

Disclosure of conflict of interest

The authors declare no competing interests.

Statement of ethical approval

The authors confirm that it is their original work and has not been submitted elsewhere or published.

Author's Contribution

Dr. Vikal Saxena and Dr. Rajkumar Singh made the original manuscript.

Availability of data and Materials

Data made available at request.

Author Declaration

We, the authors, affirm that this paper was composed entirely by human beings and that no AI-driven writing technologies or automated systems were used during its preparation.

References

[1] Naoki Nitta, Feixiang Wu, Jung Tae Lee, Gleb Yushin, Li-ion battery materials: present and future, Materials Today, 18(5), 2015, 252–264, https://doi.org/10.1016/j.mattod.2014.10.040.

[2] Abhay P. Srivastava; Anjani K. Pandey; Brijesh K. Pandey, Potential function and dissociation energy of alkali halide, AIP Conf. Proc. 1728, 020027 (2016), https://doi.org/10.1063/1.4946077.

[3] [3] M.M. Hasan, R. Haque, M.I. Jahirul, M.G. Rasul, I.M.R. Fattah, N.M.S. Hassan, M. Mofijur, Advancing energy storage: The future trajectory of lithium-ion battery technologies, Journal of Energy Storage, 120, 2025, 116511, https://doi.org/10.1016/j.est.2025.116511.

[4] Abhay. P. Srivastava, B.K. Pandey, A constructive approach to formulating pressure-dependent binding energy using the equation of state. Ionics (2025). https://doi.org/10.1007/s11581-025-06183-7.

[5] Pandey A. K. and Srivastava A. P., Theoretical prediction of Debye temperature for mantle minerals at high temperatures, International J. Modern Phys. B, 25(12), 1593-1600, 2011. https://doi.org/10.1142/S0217979211100175.

[6] Frith, J.T., Lacey, M.J. & Ulissi, U. A non-academic perspective on the future of lithium-based batteries. Nat Commun 14, 420 (2023). https://doi.org/10.1038/s41467-023-35933-2.

[7] Kim, H.-J.; Krishna, T.; Zeb, K.; Rajangam, V.; Gopi, C.V.V.M.; Sambasivam, S.; Raghavendra, K.V.G.; Obaidat, I.M. A Comprehensive Review of Li-Ion Battery Materials and Their Recycling Techniques. Electronics 2020, 9, 1161, https://doi.org/10.3390/electronics9071161.

[8] Abhay P. Srivastava, Brijesh K. Pandey, Anod Kumar Singh, Reetesh Srivastava, A New Fourth Order Compression Dependent Equation of State, East European Journal of Physics (2025)1, 332-339, https://doi.org/10.26565/2312-4334-2025-1-40.

[9] Valizadeh, A., Amirhosseini, M.H. Machine Learning in Lithium-Ion Battery: Applications, Challenges, and Future Trends. SN COMPUT. SCI. 5, 717 (2024). https://doi.org/10.1007/s42979-024-03046-2.

[10] J. Mitali, S. Dhinakaran, A.A. Mohamad, Energy storage systems: a review, Energy Storage and Saving, 1(3), 2022, 166–216, https://doi.org/10.1016/j.enss.2022.07.002.

[11] Aghmadi, A.; Mohammed, O.A. Energy Storage Systems: Technologies and High-Power Applications. Batteries 2024, 10, 141. https://doi.org/10.3390/batteries10040141.

[12] Abhay P. Srivastava, Brijesh K. Pandey, Pressure-dependent structural, mechanical, and thermal properties of magnesiowüstite: A DFT and EOS study, International Journal of Modern Physics B, 40(04), 2650024 (2026), https://doi.org/10.1142/S0217979226500244.

[13] Maurya, D., Pandey, B.K. & Srivastava, A.P. Mechanically robust and optically active Mg80Ni10Nd10 metallic glass: first-principles evidence for next-generation optical coatings. Opt Quant Electron 58, 28 (2026). https://doi.org/10.1007/s11082-025-08615-0.

[14] Abhay P. Srivastava, Brijesh K. Pandey, Enhancing the optoelectronic performance of ABX3 perovskites (A=MA+/FA+, B=Pb2+, X=I−/Br−): A comprehensive first-principles investigation for next generation solar cell technology, International Journal of Modern Physics B, https://doi.org/10.1142/S0217979225502923.

[15] Srivastava, A. Prakash, Pandey, B. Kumar, and Shanker, A. (2025). Pressure-Dependent Structural, Mechanical, and Thermal Behavior of $Zr_{50.5}Ti_{4.8}Cu_{19.0}Ni_{11.4}Al_{14.3}$ Bulk Metallic Glass: A DFT and Equation of State Study. (e234974). Physical Chemistry Research, (14), e234974 https://doi.org/10.22036/pcr.2025.552725.2766.

[16] [16] Perdew, J. P., Burke, K., & Ernzerhof, M. (1996). Generalized Gradient Approximation Made Simple. Physical Review Letters, 77(18), 3865. https://doi.org/10.1103/PhysRevLett.77.3865.

[17] Blöchl, P. E. (1994). Projector augmented-wave method. Physical Review B, 50(24), 17953. https://doi.org/10.1103/PhysRevB.50.17953.

[18] Henkelman, G., Uberuaga, B. P., & Jónsson, H. (2000). A climbing image nudged elastic band method for finding saddle points and minimum energy paths. The Journal of Chemical Physics, 113(22), 9901–9904. https://doi.org/10.1063/1.1329672.

[19] Ohzuku, T., Ueda, A., & Nagayama, M. (1993). Electrochemistry and structural chemistry of LiNiO2 (R3m) for 4-volt secondary lithium cells. Journal of the Electrochemical Society, 140(7), 1862–1870. https://doi.org/10.1149/1.2220729.

[20] Yazami, R., & Touzain, P. (1983). A reversible graphite-lithium negative electrode for electrochemical generators. Journal of Power Sources, 9(3), 365–371. https://doi.org/10.1016/0378-7753(83)80007-8.

[21] Xu, B., Qian, D., Wang, Z., & Meng, Y. S. (2012). Recent progress in cathode materials research for advanced lithium-ion batteries. Materials Science and Engineering: R: Reports, 73(5-6), 51–65. https://doi.org/10.1016/j.mser.2012.05.003.

[22] Park, K. S., Benayad, A., Kang, D. H., & Doo, S. G. (2007). Nanosize effect on high-power and high-capacity $LiCoO_2$ cathode. Electrochemical and Solid-State Letters, 10(8), A223–A227. https://doi.org/10.1149/1.2748345.

[23] Lee, E., Persson, K. A. (2013). Structural and chemical origin of the oxygen redox activity in layered and cation-disordered Li-excess cathode materials. Energy & Environmental Science, 6(1), 360–370. https://doi.org/10.1039/C2EE23338A.

[24] Abhay P. Srivastava, Brijesh K. Pandey, Pressure-dependent evolution of Bi2Sr2CaCu2O8+δ: DFT insights for high-pressure superconducting applications, Solid State Communications, 404, 2025, 116112, https://doi.org/10.1016/j.ssc.2025.116112.

[25] Kanno, R., & Takeda, Y. (1994). Electronic structure and lithium intercalation behavior in $LiCoO_2$. Solid State Ionics, 68(3-4), 263–267. https://doi.org/10.1016/0167-2738(94)90421-9.

[26] Srivastava, A.P., Pandey, B.K. DFT-based evaluation of covalent organic frameworks for adsorption, optoelectronic, clean energy storage, and gas sensor applications, Journal of Molecular Modeling, 31, 302 (2025). https://doi.org/10.1007/s00894-025-06535-0.

[27] Liu, Y., Fan, X., Wang, L., & Zhang, H. (2015). Effect of Al doping on $LiCoO_2$: A first-principles study. RSC Advances, 5(30), 23899–23906. https://doi.org/10.1039/C4RA16004F.

[28] Sarker, M.R.; Saad, M.H.M.; Riaz, A.; Lipu, M.S.H.; Olazagoitia, J.L. Micro Energy Storage Systems in Energy Harvesting Applications: Analytical Evaluation towards Future Research Improvement. Micromachines 2022, 13, 512. https://doi.org/10.3390/mi13040512.

[29] Aydinol, M. K., Kohan, A. F., Ceder, G., Cho, K., & Joannopoulos, J. (1997). Ab initio study of lithium intercalation in metal oxides and metal dichalcogenides. Physical Review B, 56(3), 1354. https://doi.org/10.1103/PhysRevB.56.1354.

[30] Van der Ven, A., Ceder, G. (2000). Lithium diffusion mechanisms in layered intercalation compounds. Electrochimica Acta, 45(1-2), 131–150. https://doi.org/10.1016/S0013-4686(99)00236-6.

[31] Ukoba, K., Olatunji, K. O., Adeoye, E., Jen, T.-C., & Madyira, D. M. (2024). Optimizing Renewable Energy Systems through Artificial Intelligence: A Review and Future Prospects. Energy & Environment, 35(7), 3833-3879. https://doi.org/10.1177/0958305X241256293.

[32] Abhay P. Srivastava, Brijesh K. Pandey, Abhishek K. Gupta, Explore the fascinating realm of comparing metal melting curves by applying the equation of state and Lindemann's law, Computational Condensed Matter, 40, 2024, e00952, 2352-2143, https://doi.org/10.1016/j.cocom.2024.e00952.

[33] Tong X. Research on key technologies of large-scale wind-solar hybrid grid energy storage capacity, big data configuration optimization. Wind Engineering. 2023;48(1):32-43. https://doi.org/10.1177/0309524X231188951.

[34] Mizushima, K., Jones, P. C., Wiseman, P. J., & Goodenough, J. B. (1980). $LixCoO_2$ ($0 < x \leq 1$): A new cathode material for batteries of high energy density. Materials Research Bulletin, 15(6), 783–789. https://doi.org/10.1016/0025-5408(80)90012-4.

[35] Wu, N., Zeng, X., Huang, X., & Xu, H. (2018). Enhanced lithium storage properties of V-doped $LiCoO_2$: A first-principles investigation. Journal of Power Sources, 378, 408–414. https://doi.org/10.1016/j.jpowsour.2017.12.074.

[36] Lee, J., Urban, A., Li, X., Su, D., Hautier, G., & Ceder, G. (2014). Unlocking the potential of cation-disordered oxides for rechargeable lithium batteries. Science, 343(6170), 519–522. https://doi.org/10.1126/science.1246432.

[37] Dahn, J. R., Sleigh, A. K., Shi, H., Reimers, J. N., Zhong, Q., & Way, B. M. (1994). Dependence of the electrochemical intercalation of lithium in carbon on the crystal structure of the carbon. Electrochimica Acta, 39(5), 921–928. https://doi.org/10.1016/0013-4686(94)85062-5.

[38] Yoo, E., Kim, J., Hosono, E., Zhou, H., Kudo, T., & Honma, I. (2008). Large reversible Li storage of graphene nanosheet families for use in rechargeable lithium-ion batteries. Nano Letters, 8(8), 2277–2282. https://doi.org/10.1021/nl800705t.

[39] Wang, Z., Luan, D., Madhavi, S., Hu, Y., & Lou, X. W. (2012). Assembling carbon-coated α-Fe_2O_3 hollow nanohorns on the CNT backbone for superior lithium storage capability. Energy & Environmental Science, 5(2), 5252–5256. https://doi.org/10.1039/C1EE02742C.